Sol-gel synthesis of cubic Nb/Ta-doped SrCoO3-δ with mixed nano-micro morphology

Sol-gel synthesis of cubic Nb/Ta-doped $SrCoO_{3-\delta}$ with mixed nano-micro morphology

V.C. Fuertes[a,*], F.M. Eroles[a], A.D. Menzaque[a], W.J. Peláez[a], D.G. Lamas[b]

[a]INFIQC-CONICET, Departamento de Fisicoquímica, Facultad de Ciencias Químicas, Universidad Nacional de Córdoba, Haya de la Torre S/N, Ciudad Universitaria, Córdoba (5000), Argentina.
[b]CONICET/Escuela de Ciencia y Tecnología, Universidad Nacional de General San Martín, Martín de Irigoyen 3100, Edificio Tornavía, Campus Miguelete, San Martín, Buenos Aires, Argentina.

*Corresponding author. E-mail address: vfuertes@gmail.com (V.C. Fuertes)
Phone number: +54-351-5353866 (ext. 53524); Fax number: +54-351-4334188.

Abstract

$SrCo_{0.90}M_{0.10}O_{3-\delta}$ (M= Nb, Ta) perovskite powders were synthesized by sol-gel, using tartrate-precursor decomposition. The crystal structure of these materials was analyzed by X-ray powder diffraction. Rietveld refinements showed that both samples achieved the cubic crystal structure (Pm-3m), which was stabilized by the incorporation of highly-charged transition-metal cations at the octahedral sites. This synthesis method successfully lowered the calcination temperature relative to other methods mentioned in literature. The concentration of oxygen vacancies (δ value) was determined by thermogravimetric analysis. Microstructural analysis revealed micrometric scale particles with a superficial nanometric dendritic array with an average grain size less than 100 nm. The present work provides a new strategy to synthesize nanostructured perovskite materials that could have better electrical and electrochemical properties.

Keywords

Sol-gel synthesis; Perovskites; X-ray analysis; Mixed microstructure; Dendritic habit; Fuel cells.

1. Introduction

Currently, solid oxide fuel cells (SOFCs) are one of the most promising electrochemical devices developed for energy conversion **[1]**. These devices, however, may present complex problems such as electrode degradation and interfacial reactions between the electrolyte and the electrodes due to their high operating temperatures, above 1000 °C **[2]**. To avoid these problems, it is desirable to operate SOFCs at temperatures between 500-800 ºC **[2,3]**, known as 'intermediate-temperature solid-oxide fuel cells' (IT-SOFCs). Nonetheless, intermediate temperatures affect the performance of the cathode, which is responsible for catalyzing the reduction of $O_{2(g)}$ to oxide ions (O^{2-}). As the temperature decreases, the cathode presents a significant drop of its electrochemical response, thus decreasing the energy density of the device. One of the main improvements required for the commercialization of IT-SOFCs is the development of new mixed ionic-electronic conductors (MIECs) that confer a better performance at intermediate temperatures **[4,5,6]**. MIECs materials provide not only the electrons for the reduction of oxygen but also the ionic conduction required to ensure the transport of the formed oxide ions **[7]**. This allows the oxygen reduction reaction to take place on the entire surface of the electrode, unlike conventional electronic conductors in which the reaction occurs only on the triple points [electrolyte / electrode / gas] **[7]**. Pioneer research on MIEC cathodes for IT-SOFCs is focused on the search of perovskite-type structures that combine high tolerance to oxygen vacancies, electronic conductivity and electrochemical activity for oxygen reduction **[4,8,9]**.

$SrCoO_{3-\delta}$–based perovskites are promising candidates to fulfill this role because they are MIECs with high ionic conductivity **[10-12,13,14]**. Particularly, the cubic-3C phase of $SrCoO_{3-\delta}$ is of great interest as it offers high O^{2-}-conductivity due to its corner-linked octahedral network while the cubic structure vacancies allow for an oxygen permeation

flux **[15-17]**. Unfortunately, this phase is not stable at temperatures lower than 900 °C and suffers a transition to a dielectric hexagonal-2H phase **[16]**.

Nevertheless, the high-temperature cubic phase can be retained at lower temperatures, and even at room temperature, by partially doping the cobalt site with other transition metal cations (usually tetra-, penta- or hexavalent). The inclusion of a highly charged cation at the octahedral position induces electrostatic repulsion effects that destabilize the octahedral face-sharing configuration present in the 2H hexagonal phase **[18]**. Hence, the phase transition can be avoided by generating a solid solution of the type $SrCo_{1-x}M_xO_{3-\delta}$ where the incorporation of M^{n+} cations stabilizes the new phase. In this framework, there are several articles analyzing the effect of partial substitutions of cobalt by Ti^{4+} **[3]**, V^{5+} **[3]**, Nb^{5+} **[17]**, Sb^{5+} **[18]**, Mo^{6+} **[19]** or Ta^{5+} **[20]** ions, in which the stabilization of the cubic phase at room temperature is reported.

Particularly, the incorporation of Nb^{5+} and Ta^{5+} ions at the Co positions in the $SrCo_{1-x}M_xO_{3-\delta}$ system was recently reported by Cascos et al. **[21]** and Chen et al. **[20]**, showing that these ions promote the stabilization of a tetragonal superstructure and cubic phase, respectively. However, these materials were synthesized by methods that employed high temperatures, generating crystallite sizes on a micrometric scale **[17,20,21]**.

No wet chemistry method for the synthesis of cubic Nb/Ta-doped $SrCoO_{3-\delta}$ perovskites has been reported to date. Based on this context, the present study is focused on the synthesis of cubic $SrCo_{0.90}M_{0.10}O_{3-\delta}$ perovskites (with M= Nb^{5+} and Ta^{5+}), using temperatures lower than those already reported in the above-mentioned works. Specifically, a tartrate-decomposition sol-gel method was employed. The materials developed in this work were characterized with X-ray powder diffraction, thermal gravimetric analysis, spectroscopic and microscopic measurements.

2. Materials and Methods

$SrCo_{0.90}M_{0.10}O_{3-\delta}$ (M= Nb, Ta) powders were prepared from metal nitrates of analytical grade with $Nb_2O_{5(s)}$ or $Ta_2O_{5(s)}$ as precursors of the doping ions. A dissolution treatment was necessary to synthesize the samples because the oxides of niobium and tantalum are insoluble in water, even with small aggregates of $HNO_{3(ac)}$. Hydrofluoric acid (48-51% W / V), ammonia (28-30% W / V), hydrogen peroxide (30% W / V) and $(NH_4)_2C_2O_4 \bullet H_2O_{(s)}$ were used in order to carry out the dissolution process of niobium and tantalum oxides.

2.1. $Nb_2O_{5(s)}$ y $Ta_2O_{5(s)}$ dissolution

The dissolution of $M_2O_{5(s)}$ (M= Nb and Ta) was achieved via the formation of a soluble complex of the corresponding metallic tartrates **[22]**. The $M_2O_{5(s)}$ oxide was dissolved in HF 48–51% W/V under a heated water bath with stirring. When the complete dissolution of the oxide was reached, the heating was halted and a solution of ammonium oxalate was added to regulate pH. The precipitation of a hydrated oxide was then produced by the continuous dripping of ammonia into the solution, under an ice bath. The precipitate was filtered and washed with ammonia solution to ensure the complete elimination of fluorine. Finally, the required quantity of hydrated oxide was dissolved with tartaric acid and continuous additions of hydrogen peroxide, under heating with constant stirring, until complete dissolution (yellow colored for niobium and white for tantalum). A complete summary of the procedure is detailed in **Figure 1**.

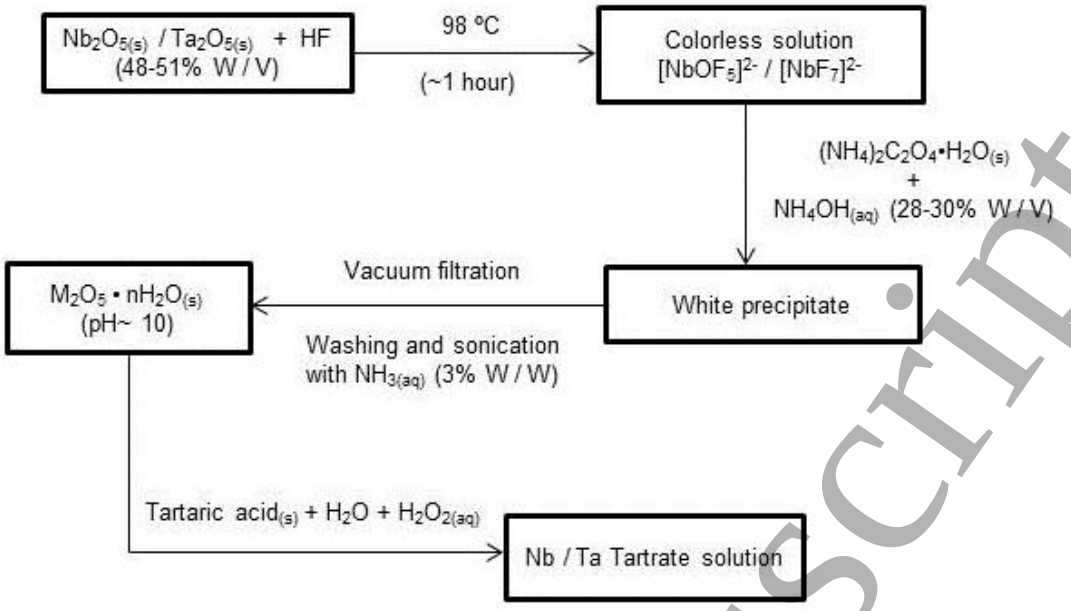

Figure 1. Dissolution process of $Nb_2O_{5(s)}$/$Ta_2O_{5(s)}$, resulting in the formation of a soluble complex of the corresponding metal tartrate.

2.2. Sol-gel synthesis

The synthesis of samples was carried out using the sol-gel method. Stoichiometric quantities of the strontium and cobalt nitrates were dissolved along with the appropriate amount of Nb/Ta tartrate solution. Solid tartaric acid (a complexing agent) was added in a molar ratio equivalent to twice the total cations, and ethylene glycol (a polymerization agent) in a 1:3 ratio in relation to tartaric acid. The resulting solutions were thermally treated, with magnetic stirring, until the formation of a vermilion precursor gel. The resulting gel was treated following a three-stage procedure: 100 ºC for 2 hours (to evaporate the remaining water), 300 ºC for 3 hours and 600 ºC for 12 hours (to eliminate nitrates and remains of organic matter through the formation of $CO_{2(g)}$ and $NO_{2(g)}$). The resulting black precursor was calcined in air atmosphere for 36 hours (48 hours for Ta-doped sample) in subsequent heat treatments at increasing temperatures until the highest degree of purity was achieved. The final calcination temperatures were of 975 ºC and 1075 ºC for the Nb-doped and Ta-doped samples, respectively. Two samples of each composition were synthesized, demonstrating the versatility and good reproducibility of the method.

2.3. Characterization

The structural characterization of the products was carried out by X-ray powder diffraction (XRPD) using a PANalytical X-ray diffractometer model X' Pert Pro with PIXcel detector (40 kV, 40 mA) with a graphite monochromator, in Bragg-Brentano reflection geometry with CuKα radiation (λ = 1.5418 Å). The 2θ range was of 15-100° in steps of 0.02°. The refinement of the crystal structures was performed by the Rietveld method **[23]** using the FULLPROF program **[24]**. A pseudo-Voigt shape function was used.

Infrared spectroscopy with Fourier transform (FT-IR) studies were also carried out using a Brüker IFS-28 FT-IR spectrometer, in the range between 4000-400 cm^{-1}, with a spectral resolution of 2 cm^{-1}. Furthermore, Raman spectroscopy was used to probe the symmetry of the crystal structure of synthesized samples. Raman spectra were obtained with a HORIBA spectrometer model LabRAM HR 800, using a green laser of λ= 514.5 nm and a power of 4 mW with diffraction grating of 600 lines / mm.

Thermogravimetric analyses were carried out to determine the oxygen vacancies (δ) in the samples with a Shimadzu DTG-60 device in air flow up to 900 °C, using a heating rate of 10 ºC/min with α-alumina as reference and crucible material **[21,25]**. The morphology of the samples was observed by field-emission scanning electron microscopy (FE-SEM) images using a Zeiss Sigma FE-SEM microscope.

3. Results and Discussion

3.1. XRPD analysis

Figure 2 shows XRPD patterns at room temperature for the a) $SrCo_{0.90}Nb_{0.10}O_{3-\delta}$ sample synthesized at 900 ºC, 950 ºC and 975 ºC, and b) $SrCo_{0.90}Ta_{0.10}O_{3-\delta}$ sample heat-treated at 1000 ºC, 1050 ºC and 1075 ºC. For the Nb-doped sample calcined at 900 ºC, it was observed that the main phase correlated to a cubic perovskite-type one with the presence of an orthorhombic (brownmillerite) phase (ICSD #162239) **[26]** and a hexagonal phase (ICSD #427011) **[27]**, and a rhombohedral phase (ICSD #81312) as impurities. In addition, the small peak present at ~31º in 2θ, is probably due to a residue of Co_3O_4 (ICSD #27497). A decrease of the intensity of the peaks corresponding to these secondary phases was seen with successive thermal treatments until a final heating step of 975 ºC, where the sample exhibited a single-phase perovskite. In the case of the $SrCo_{0.90}Ta_{0.10}O_{3-\delta}$ sample, it was necessary to raise the calcination temperature to 1075 ºC to increase its purity.

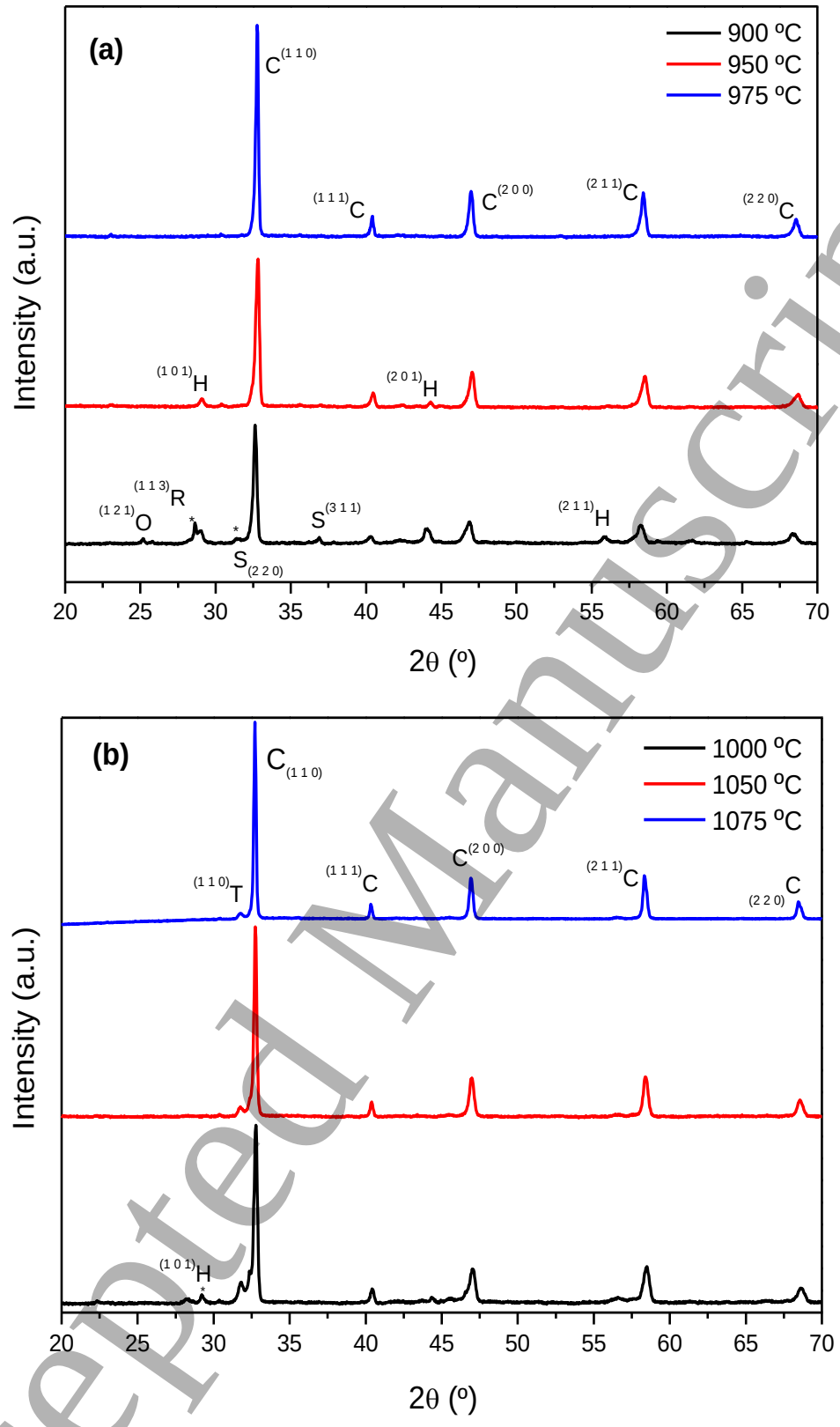

Figure 2. X-ray powder diffraction patterns for a) $SrCo_{0.90}Nb_{0.10}O_{3-\delta}$ and b) $SrCo_{0.90}Ta_{0.10}O_{3-\delta}$, calcined at increasing temperatures. Each diffraction peak has been labeled indicating the main and secondary phases present in the samples, where C: cubic

phase, H: hexagonal phase, O: orthorhombic phase, T: tetragonal phase, R: rhombohedral phase, S: Spinel Co_3O_4.

Rietveld analysis of XRPD data for both final samples ($SrCo_{0.90}Nb_{0.10}O_{3-\delta}$ calcined at 975 °C and $SrCo_{0.90}Ta_{0.10}O_{3-\delta}$ calcined at 1075 °C) was performed using the crystal structure data reported in the ICSD ("Inorganic Crystal Structure Database") database. For these refinements, tetragonal P4/mmm (ICSD# 238964) and cubic Pm-3m (ICSD# 190750) models with similar structure to those reported in literature were used **[17,20,21]**. Knowledge of the crystal structure of these materials is important to understand their potential application as an IT-SOFC cathode. It is important to determine the distribution of oxygen vacancies or the spatial dispositions of the atoms in the crystal lattice, as they are directly related to the electrochemical performance. A tetragonal crystal superstructure would locate the oxygen vacancies on a single plane of $(Co/M)O_6$ octahedra **[17,21]**, whereas the cubic phase would have the vacancies distributed homogeneously throughout the material, thus increasing its ionic conductivity in all directions **[16]**.

Both models would explain all peaks present in the XRPD patterns of both samples. However, the tetragonal model assigns a peak (centered on ~25.6º in 2θ) which was not detected in the experimental pattern, indicating that this structural model is inadequate for these samples. Further discrepancies can be seen in the amplified range near ~68.5º in 2θ shown in **Figure 3**. Here it can be observed that the cubic model better fits the experimental data, suggesting two overlapping peaks rather than an asymmetric peak. Thus, the Rietveld analysis confirms that the main diffraction peaks can be well indexed according to a cubic perovskite structure with Pm-3m space group. Therefore, these results show that the sol-gel method reported in the present work (tartrate-precursor decomposition) successfully lowered the calcination temperature by 225 ºC for the Nb-

doped sample and by 125 ºC for the Ta-doped sample, with respect to traditional solid-state syntheses of these materials **[20,28]**.

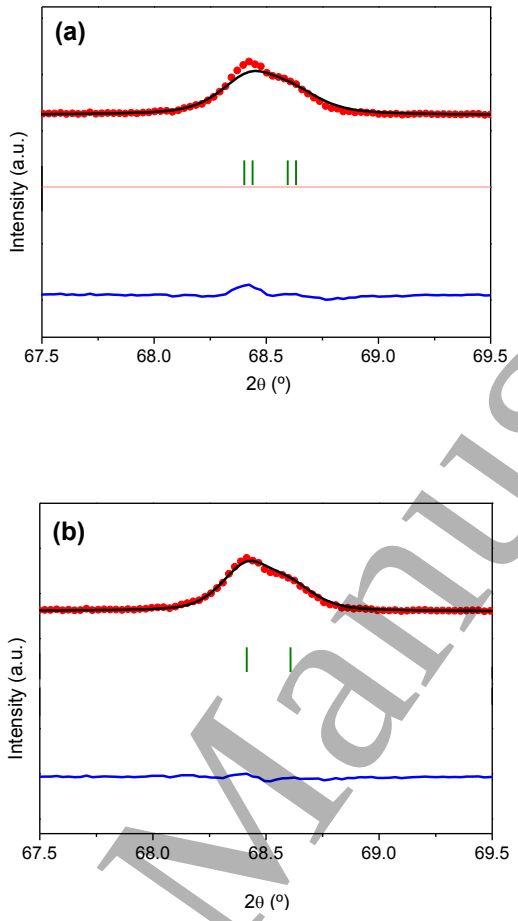

Figure 3. Rietveld refinements in the amplified 2θ range near ~68.5º using: a) a tetragonal model (P4/mmm space group) vs b) a cubic model (Pm-3m space group) for $SrCo_{0.90}Nb_{0.10}O_{3-\delta}$ calcined at 975 ºC.

Rietveld refinements of XRPD patterns at RT for both samples are presented in **Figure 4**. The *a* parameters of the Nb-doped and Ta-doped samples resulted of 3.8726(2) Å and 3.8762(1) Å, respectively. No impurity phases were detected in the $SrCo_{0.90}Nb_{0.10}O_{3-\delta}$ sample while the $SrCo_{0.90}Ta_{0.10}O_{3-\delta}$ sample was obtained with a small impurity of a tetragonal phase (ICSD# 028918), shown in the second group of Bragg's reflections. Using the information obtained from these Rietveld refinements, a representation of the structural arrangement of the ions in the crystal lattice was

generated by the *Vesta 3.1.8* program **[29]** as presented in **Figure 4 (see inset)**. It can be observed in this figure that the $(Co/M)O_6$ octahedra are joined through their vertices, creating a compact packed lattice in which Sr^{2+} ions are placed between octahedra.

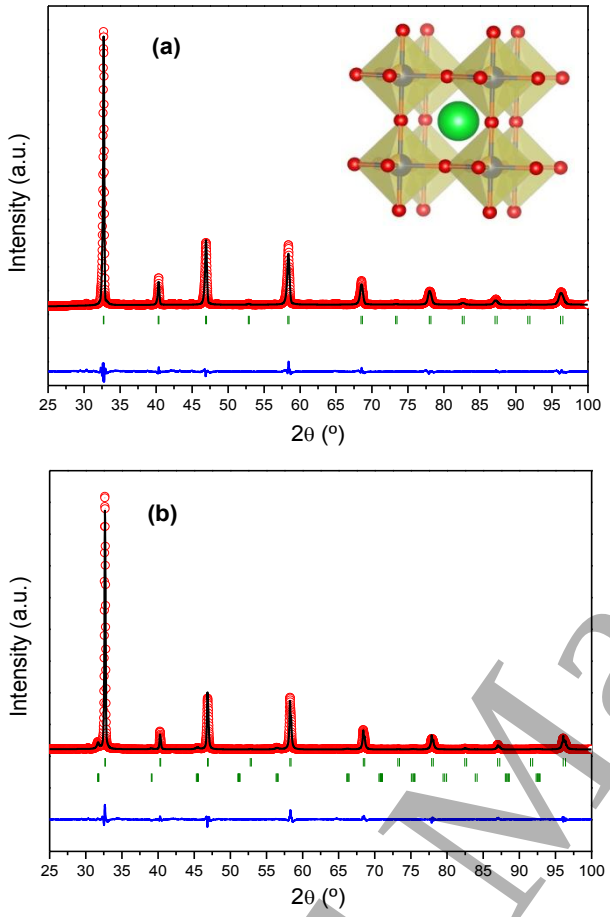

Figure 4. Rietveld refinement of XRPD patterns for a) $SrCo_{0.90}Nb_{0.10}O_{3-\delta}$ (discrepancy factors: χ^2= 19.1, R_{wp}= 3.95, R_p= 2.72, R_{Bragg}= 3.28) and b) $SrCo_{0.90}Ta_{0.10}O_{3-\delta}$ (discrepancy factors: χ^2= 32.0, R_{wp}= 4.85, R_p= 3.20, R_{Bragg}= 2.80). *Inset:* Cubic crystal structure proposed for $SrCo_{0.90}M_{0.10}O_{3-\delta}$ where strontium is shown in green spheres, cobalt/dopant in blue/orange spheres and oxygen in red spheres.

3.2. FT-IR and Raman spectroscopy

To complement the XRPD study, FT-IR analysis of $SrCo_{0.90}Nb_{0.10}O_{3-\delta}$ and $SrCo_{0.90}Ta_{0.10}O_{3-\delta}$ samples was also carried out. Perovskite-type oxides have an intense band at ~600 cm^{-1}, attributed to the asymmetric M–O stretch of the MO_6 octahedra,

where M represents the transition metal **[30]**. The spectra obtained for these samples are presented in **Figure 5**, bounded between 400 and 4000 cm^{-1}. It can be observed in this figure that both samples presented an intense band centered at 580 cm^{-1}, which is due to the stretching vibrations of the MO_6 octahedra. The small absorption peaks around 2343 cm^{-1}, 2847 cm^{-1} and 2921 cm^{-1} present in the Ta-doped sample are due to CO_2 molecules present in air and to the symmetric and antisymmetric stretching of C–H bonds, respectively. It should be pointed out here that the presence of such bands has not been considered as contamination of the sample, but may be related to residual organic matter. A broad absorption band at ~3400 cm^{-1} is attributed to the hydroxyl (−OH) group of H_2O, indicating the existence of water absorbed on the surface of the sample.

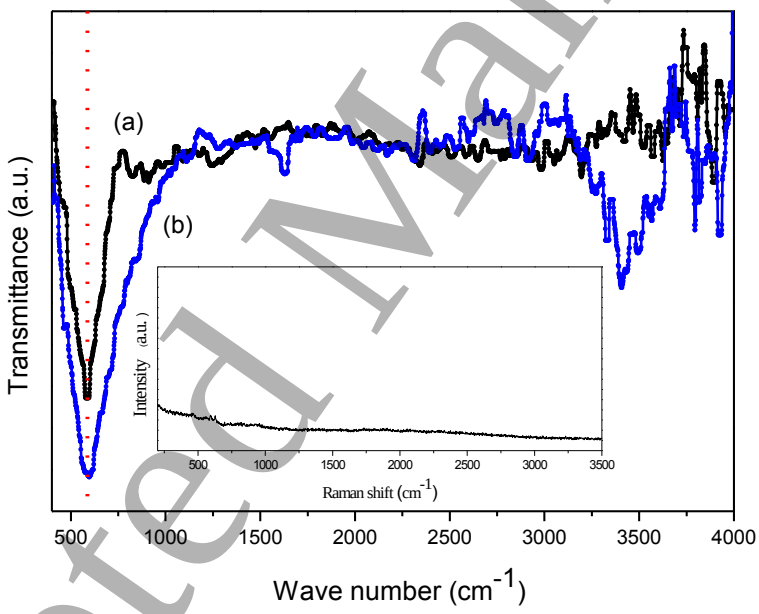

Figure 5. FT-IR spectra for a) $SrCo_{0.90}Nb_{0.10}O_{3-\delta}$ and b) $SrCo_{0.90}Ta_{0.10}O_{3-\delta}$. The intense band at ~580 cm^{-1} is characteristic of Perovskite-type oxides. *Inset:* Raman spectra for $SrCo_{0.90}Ta_{0.10}O_{3-\delta}$.

Additionally, a Raman analysis was performed to revalidate that the samples present a cubic phase. Using a group theory analysis, Sacchetti et al. predicted that a cubic

structure of solids of similar composition should not have any active modes in Raman **[31]**. In this framework, Zhu et al. reported that a tetragonal P4/mmm structure of Nb-doped strontium cobaltite samples exhibit six active modes in Raman while a cubic Pm-3m one does not present any active mode **[28]**. The spectrum obtained is presented in **Figure 5 (see inset)**, bounded between 400 and 3500 cm^{-1}. Analyzing this spectrum, the lack of active phonon peaks confirmed that the samples present a cubic structure. Weak signals observed at ~650 cm^{-1} are attributed **[31]** to Raman prohibited modes that are activated by disorder in the crystal lattice, or by second order Raman scattering, and not by the presence of a significant tetragonal phase.

3.3. Thermal gravimetric analysis

The TGA curves obtained for these samples are shown in **Figure 6**. A pronounced and continuous loss of mass was observed for temperatures higher than 350 ºC, for both samples. A weight loss equivalent to 1.19% and 1.17% is seen for $SrCo_{0.90}Nb_{0.10}O_{3-\delta}$ and $SrCo_{0.90}Ta_{0.10}O_{3-\delta}$, respectively, at 850 ºC. No thermodynamic process was present in the differential thermic analysis (DTA) (not shown), as such the weight change is completely attributed to oxygen loss. Consequently, an oxygen non-stoichiometry of δ= 0.15 was calculated for both samples. This allowed the chemical formulas to be rewritten as: $SrCo_{0.90}Nb_{0.10}O_{2.85}$ and $SrCo_{0.90}Ta_{0.10}O_{2.85}$. Assuming an oxidation state of 5+ for Nb and Ta cations in the structure, an average oxidation state of 3.56+ was obtained for Co cations in both samples. These analyses indicated that, under IT-SOFC working conditions, the materials are oxygen deficient improving the movement of O^{2-} through these MIEC oxides **[17]**. After the thermogravimetric analysis, the XRPD patterns of the residual solids were measured and resulted indistinguishable from the starting patterns. This confirms no decomposition or phase transitions after heating in air, and suggests a complete reversibility of the absorption-desorption oxygen process.

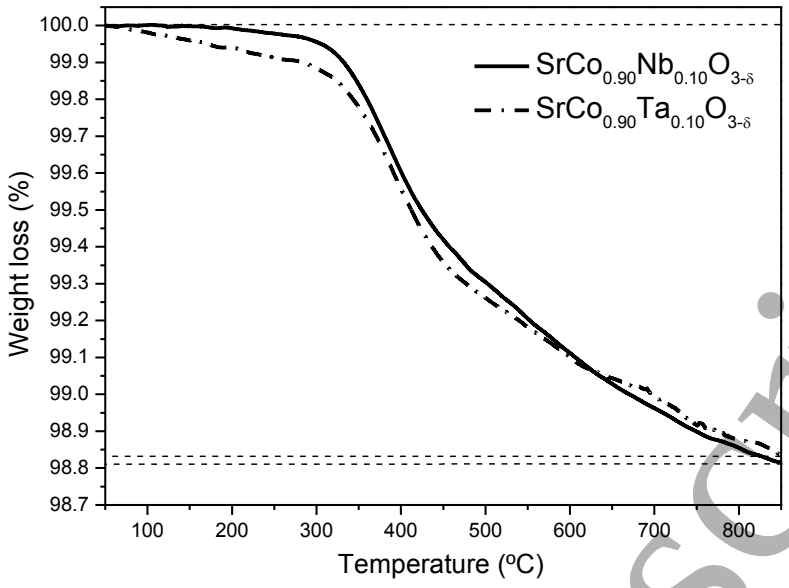

Figure 6. TGA curves for $SrCo_{0.90}Nb_{0.10}O_{3-\delta}$ (bold) and $SrCo_{0.90}Ta_{0.10}O_{3-\delta}$ (dashed) in air flow.

3.4. Microstructural analysis

The morphology of the samples obtained after the final calcination treatment was analyzed by FE-SEM, as shown in **Figure 7**. Micrometric particles of approximately 2 μm can be observed in both cases. Furthermore, a nanometric dendritic habit can be seen evenly distributed over the whole surface of each sample, with an average grain size less than 100 nm.

Previous solid state syntheses of these materials have resulted in similar micrometric-sized particles **[20,28]**, although none have been reported to exhibit a superficial nanometric habit. This is to be expected, as this method of synthesis is known to yield products with higher particle size and low surface area **[32]**. However, wet chemistry routes of synthesis, like the sol-gel method, are known not only to reduce calcination temperature but also to produce nanomaterials **[32]**. Therefore, the novel nano-morphology observed is attributed to the tartrate-precursor decomposition sol-gel method employed.

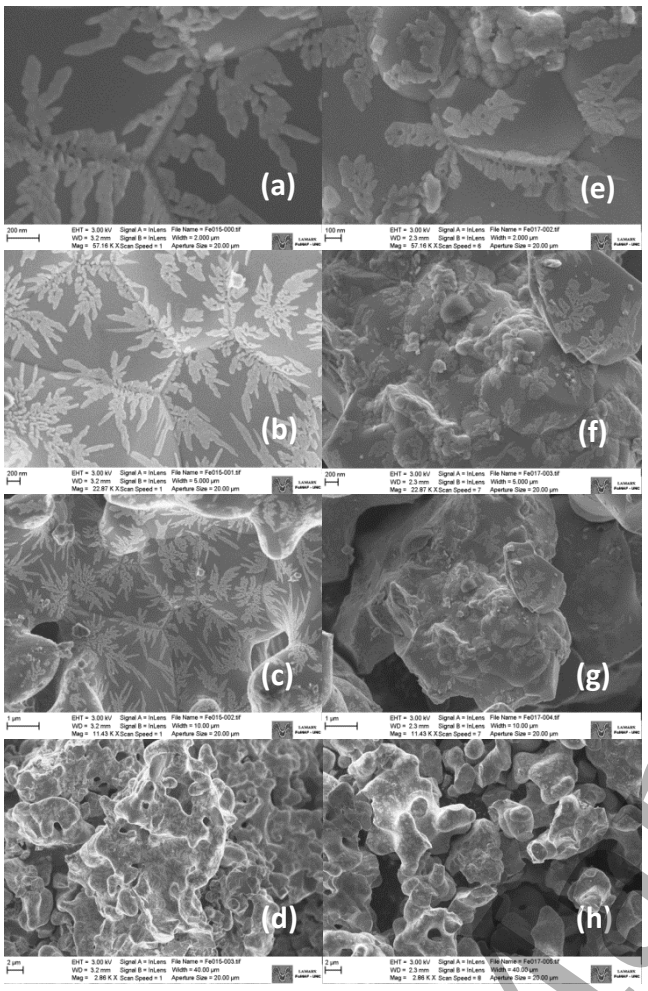

Figure 7. FE-SEM images with decreasing magnifications for the samples obtained after the final calcination treatment: a-d) $SrCo_{0.90}Nb_{0.10}O_{2.85}$ calcined at 975 °C and e-h) $SrCo_{0.90}Ta_{0.10}O_{2.85}$ calcined at 1075 °C.

A mixed nano-micro surface brings forth a new prospect for the construction of IT-SOFC electrodes. This new nano-component could give the electrode a high density of defects (grain edges, polyoriented edges, punctual defects, etc.) and greater surface area which could lead to an improvement of previously measured electrochemical properties **[28,32,5,6]**.

4. Conclusions

In summary, the incorporation of Nb^{5+}/Ta^{5+} as dopant ions allowed the stabilization of a Pm-3m cubic phase in $SrCo_{0.90}M_{0.10}O_{2.85}$ perovskites. The use of the tartrate-

precursor decomposition sol-gel method successfully lowered the synthesis temperature by 225 ºC for the Nb-doped sample and 125 ºC for the Ta-doped sample. Unlike the morphology reported for samples synthesized by the solid-state method, this method presented micrometric particles along with a novel surface nanometric dendritic habit. This change in morphology is tied to an increase in the surface/volume ratio that could prove useful in a SOFC electrode. To the best of our knowledge, this marks the first instance that a doped cubic phase $SrCoO_3$ perovskite with mixed nano-micro morphology has been synthesized by a wet chemistry method.

Acknowledgement

This work was supported by SeCyT of the Universidad Nacional de Córdoba (313/16) and Agencia Nacional de Promoción Científica y Tecnológica (PICT 2015 No. 3411). The authors thank Dr. V. Brunetti and Dr. N. Bajales Luna for their assistance in FE-SEM.

References

[1] Kendall K, Kendall M, *High-Temperature solid oxide fuel cells for the 21st century: Fundamentals, Design and Applications*, 2nd ed., Academic Press: Cambridge, MA, USA, 2015, pp. 1-24, 2016.

[2] Schrodl N, Bucher E, Egger A, Kreiml P, Teichert C, Hoschen T, Sitte W, Long-term stability of the IT-SOFC cathode materials $La_{0.6}Sr_{0.4}CoO_{3-\delta}$ and $La_2NiO_{4+\delta}$ against combined chromium and silicon poisoning, *Solid State Ion.* **276** (2015) 62-71.

[3] Cascos V, Troncoso L, Alonso J A, New families of M^{n+}-doped $SrCo_{1-x}M_xO_{3-\delta}$ perovskites performing as cathodes in solid-oxide fuel cells, *Inter. J. Hydr. Energy* **40** (2015) 134.

[4] Jun A, Kim J, Shin J, Kim G, Perovskite as a Cathode Material: A Review of its Role in Solid-Oxide Fuel Cell Technology, *ChemElectroChem* **3(4)** (2016) 511-530.

[5] Mejía Gómez A E, Sacanell J, Leyva A G, Lamas D G, Performance of $La_{0.6}Sr_{0.4}Co_{1-y}Fe_yO_3$ (y= 0.2, 0.5 and 0.8) nanostructured cathodes for intermediate-temperature solid-oxide fuel cells: Influence of microstructure and composition, *Ceramics International* **42** (2016) 3145-3153.

[6] Mejía Gómez A E, Lamas D G, Leyva A G, Sacanell J, Nanostructured $La_{0.5}Ba_{0.5}CoO_3$ as cathode for solid oxide fuel cells, *Ceramics International* **45** (2019) 14182-14187.

[7] Aguadero A, Faucett L, Taub S, Wolley R, Wu K T, Xu N, et al., Materials development for intermediate-temperature solid oxide electrochemical devices, *J. Mater. Sci.* **47** (2012) 3925-48.

[8] Zhu X, Zhai L, Gao X, Li A, An H, A novel cathode material $Pr_{0.9}Sr_{0.1}Cr_{0.5}Fe_{0.5}O_{3-\delta}$ for intermediate temperate solid oxide fuel cell, *Mater. Res. Express* **5(12)** (2018) 126307.

[9] Thenmozhi N, Sasikumar S, Sonai S, Saravanan R, Electronic structure and chemical bonding in $La_{1-x}Sr_xMnO_3$ perovskite ceramics, *Mater. Res. Express* **4(4)** (2017) 046103.

[10] Nagai T, Ito W, Sakon T R, Relationship between cation substitution and stability of perovskite structure in $SrCoO_{3-\delta}$-based mixed conductors, *Solid State Ion.* **177** (2007) 3433-3444.

[11] Deng Z Q, Liu W, Chen C S, Lu H, Yang W S, Germanium and iron Co-substituted $SrCoO_{2.5+\delta}$ as oxygen permeable membrane, *Solid State Ion.* **170** (2004) 187-190.

[12] Zeng P, Ran R, Chen Z, Zhou W, Gu H, Shao Z, Liu S, Efficient stabilization of cubic perovskite $SrCoO_{3-\delta}$ by B-site low concentration scandium doping combined with sol–gel synthesis, *J. Alloys Compd.* **455** (2008) 465-470.

[13] Jiang S P, Development of lanthanum strontium cobalt ferrite perovskite electrodes of solid oxide fuel cells–A review, *International Journal of Hydrogen Energy* (2019). Article in Press. Doi: 10.1016/j.ijhydene.2019.01.212.

[14] Wang Z, Yang Z, Song Y, Mao J, Liang F, Zhou W, Alkaline metal doped strontium cobalt ferrite perovskites as cathodes for intermediate-temperature solid oxide fuel cells, *International Journal of Hydrogen Energy* **43(29)** (2018) 13420-13429.

[15] Deng Z Q, Yang W S, Liu W, Chen C S, Relationship between transport properties and phase transformations in mixed-conducting oxides, *J. Solid State Chem.* **179** (2006) 362-369.

[16] De la Calle C, Aguadero A, Alonso J A, Fernández-Díaz M T, Correlation between reconstructive phase transitions and transport properties from $SrCoO_{2.5}$ brownmillerite: A neutron diffraction study, *Solid State Sci.* **10** (2008) 1924-1935.

[17] Cascos V, Martínez-Coronado R, Alonso J A, New Nb-doped $SrCo_{1-x}Nb_xO_{3-\delta}$ perovskites performing as cathodes in solid-oxide fuel cells, *Inter. J. Hydr. Energy* **39** (2014) 14349-54.

[18] Aguadero A, Alonso J A, Pérez-Coll D, De la Calle C, Fernández-Díaz M T, Goodenough J B, $SrCo_{0.95}Sb_{0.05}O_{3-\delta}$ as cathode material for high power density solid oxide fuel cells, *Chem. Mater.* **22** (2010) 789-798.

[19] Wang R, Jin F, Ta L, He T, $SrCo_{1-x}Mo_xO_{3-\delta}$ perovskites as cathode materials for $LaGaO_3$-based intermediate-temperature solid oxide fuel cells, *Solid State Ion.* **288** (2015) 32-35.

[20] Chen X, Huang L, Wei Y, Wang H, Tantalum stabilized $SrCoO_{3-\delta}$ perovskite membrane for oxygen separation, *J. Membrane Science* **368** (2011) 159-164.

[21] Cascos V, Alonso J A, Fernández-Díaz M T, Nb^{5+}-doped $SrCoO_{3-\delta}$ perovskites as potential cathodes for solid-oxide fuel cells, *Materials* **9** (2016) 579.

[22] Fuertes V C, Blanco M C, Franco D G, De Paoli J M, Sánchez R D, Carbonio R E, Influence of the B-site ordering on the magnetic properties of the new $La_3Co_2MO_9$ double perovskites with M = Nb or Ta, *Mater. Res. Bull.* **46** (2011) 62-69.

[23] Rietveld H M, A profile refinement method for nuclear and magnetic structures, *J. Appl. Crystallogr.* **2** (1969) 65.

[24] Rodríguez-Carvajal J, Recent advances in magnetic structure determination by neutron powder diffraction, *Physica B: Physics of Condensed Matter* **192** (1993) 55-69.

[25] Wang J, Jiang L, Xiong X, Zhang C, Jin X, Lei L, Huang K, A Broad Stability Investigation of Nb-Doped $SrCoO_{2.5+\delta}$ as a Reversible Oxygen Electrode for Intermediate-Temperature Solid Oxide Fuel Cells, *J. Electrochem. Soc.* **163** (2016) F891-F898.

[26] Muñoz A, de la Calle C, Alonso J A, Botta P M, Pardo V, Baldomir D, J. Rivas, Crystallographic and magnetic structure of $SrCoO_{2.5}$ brownmillerite: Neutron study coupled with band-structure calculations, *Physical Review B* **78** (2008) 054404.

[27] Zhao Q, Darriet J, Whangbo M -H, Ye L, Stackhouse C, zur Loye H -C, Intriguing Interconnections Among Phase Transition, Magnetic Moment, and Valence Disproportionation in 2H-Perovskite Related Oxides, *J. Am. Chem. Soc.* **133** (2011) 20981-20994.

[28] Zhu Y, Lin Y, Shen X, Sunarso J, Zhou W, Jiang S, Su D, Chen F, Shao Z, Influence of crystal structure on the electrochemical performance of A-site-deficient $Sr_{1-s}Nb_{0.1}Co_{0.9}O_{3-\delta}$ perovskite cathodes, *RSC Adv.* **4** (2014) 40865-40872.

[29] Momma K, Izumi F, VESTA 3 for three-dimensional visualization of crystal, volumetric and morphology data, *J. Appl. Crystallogr.* **44** (2011) 1272-1276.

[30] Pecchi G, Campos C, Peña O, Thermal stability against reduction of $LaMn_{1-y}Co_yO_3$ perovskites, *Mater. Res. Bull.* **44** (2009) 846.

[31] Sacchetti A, Baldini M, Postorino P, Martin C, Maignan A, Raman spectroscopy on cubic and hexagonal $SrMnO_3$, *J. Raman Spectrosc.* **37** (2006) 591-596.

[32] Mosa J, Aparicio M, *Sol-Gel Materials for Batteries and Fuel Cells*, in ed D. Levy and M. Zayat, The Sol-Gel Handbook, Wiley|VCH Verlag GmbH & Co. KGaA, 2015, Ch. 35, pp. 1071-1117. DOI:10.1002/9783527670819.

Figure Captions

Figure 1. Dissolution process of $Nb_2O_{5(s)}/Ta_2O_{5(s)}$, resulting in the formation of a soluble complex of the corresponding metal tartrate.

Figure 2. X-ray powder diffraction patterns for a) $SrCo_{0.90}Nb_{0.10}O_{3-\delta}$ and b) $SrCo_{0.90}Ta_{0.10}O_{3-\delta}$, calcined at increasing temperatures. Each diffraction peak has been labeled indicating the main and secondary phases present in the samples, where C: cubic phase, H: hexagonal phase, O: orthorhombic phase, T: tetragonal phase, R: rhombohedral phase, S: Spinel Co_3O_4.

Figure 3. Rietveld refinements in the amplified 2θ range near ~68.5º using: a) a tetragonal model (P4/mmm space group) vs b) a cubic model (Pm-3m space group) for $SrCo_{0.90}Nb_{0.10}O_{3-\delta}$ calcined at 975 ºC.

Figure 4. Rietveld refinement of XRPD patterns for a) $SrCo_{0.90}Nb_{0.10}O_{3-\delta}$ (discrepancy factors: χ^2= 19.1, R_{wp}= 3.95, R_p= 2.72, R_{Bragg}= 3.28) and b) $SrCo_{0.90}Ta_{0.10}O_{3-\delta}$ (discrepancy factors: χ^2= 32.0, R_{wp}= 4.85, R_p= 3.20, R_{Bragg}= 2.80). *Inset:* Cubic crystal structure proposed for $SrCo_{0.90}M_{0.10}O_{3-\delta}$ where strontium is shown in green spheres, cobalt/dopant in blue/orange spheres and oxygen in red spheres.

Figure 5. FT-IR spectra for a) $SrCo_{0.90}Nb_{0.10}O_{3-\delta}$ and b) $SrCo_{0.90}Ta_{0.10}O_{3-\delta}$. The intense band at ~580 cm^{-1} is characteristic of Perovskite-type oxides. *Inset:* Raman spectra for $SrCo_{0.90}Ta_{0.10}O_{3-\delta}$.

Figure 6. TGA curves for $SrCo_{0.90}Nb_{0.10}O_{3-\delta}$ (bold) and $SrCo_{0.90}Ta_{0.10}O_{3-\delta}$ (dashed) in air flow.

Figure 7. FE-SEM images with decreasing magnifications for the samples obtained after the final calcination treatment: a-d) $SrCo_{0.90}Nb_{0.10}O_{2.85}$ calcined at 975 °C and e-h) $SrCo_{0.90}Ta_{0.10}O_{2.85}$ calcined at 1075 °C.